THE UPPER-LEVEL STATIC STABILITY AND TROPOPAUSE STRUCTURE OF TROPICAL CYCLONES

by

Patrick Timothy Duran

A Dissertation

Submitted to the University at Albany, State University of New York

in Partial Fulfillment of

the Requirements for the Degree of

Doctor of Philosophy

College of Arts and Sciences

Department of Atmospheric and Environmental Sciences

2018

ABSTRACT

Upper-tropospheric thermodynamic processes can play an important role in tropical cyclone (TC) structure and evolution. Despite its importance, until recently few in-situ observations were available in the upper levels of TCs. Two recent field campaigns - the NASA Hurricane and Severe Storm Sentinel (HS3) and the Office of Naval Research Tropical Cyclone Intensity (TCI) experiment - provided a wealth of high-altitude observations within TCs. These observations revealed that the upper-level static stability and tropopause structure can change dramatically with both space and time in TCs.

The TCI dropsonde dataset collected during the rapid intensification (RI) of Hurricane Patricia (2015) revealed dramatic changes in tropopause height and temperature within the storm's inner core. These changes in tropopause structure were accompanied by a systematic decrease in tropopause-layer static stability over the eye. Outside of the eye, however, an initial decrease in static stability just above the tropopause was followed by an increase in static stability during the latter stages of RI.

Idealized simulations were conducted to examine the processes that might have been responsible for the tropopause variability observed in Hurricane Patricia. A static stability budget analysis revealed that three processes - differential advection, vertical gradients of radiative heating, and vertical gradients of turbulent mixing - can produce the observed variability. These results support the theoretical assumption that turbulent mixing plays a fundamental role in setting the upper-level potential temperature stratification in TCs. The existence of turbulence in the upper troposphere of TCs is corroborated by the presence of low-Richardson number layers in a large number of rawinsonde observations. These layers

were more common in hurricanes than in weaker TCs, as hurricanes were characterized by both smaller static static stability and larger vertical wind shear in the upper troposphere.

HS3 dropsondes deployed within and around TC Nadine (2012) observed two distinct upper-level stability maxima within the storm's cirrus canopy. Outside of the cirrus canopy, however, only one stability maximum was present in the upper levels. In a large rawinsonde dataset, multiple stability maxima like those observed in Nadine were observed more often within cold cirrus clouds than outside of cirrus. It is hypothesized that vertical gradients of radiative heating within cirrus clouds could produce these multiple stability maxima. MENTION THAT STABLE LAYER IS STRONGER WITHIN COLD CIRRUS AND THAT IT'S ALSO STRONGER IN HURRICANES THAN IN TD+TS?

ACKNOWLEDGEMENTS

This dissertation is the fulfillment of a childhood dream that would not have come true without the selfless dedication of countless people.

First I must thank my advisor, John Molinari, for his unswerving kindness, humility, and patience over these past six years. Former students have described him as a "brilliant scientist and an even better man," an assessment with which I wholeheartedly concur. I could not have asked for a better mentor, and am so grateful for the opportunities he has given to me.

I also would like to thank my committee members - Kristen Corbosiero, Robert Fovell, Brian Tang, and Ryan Torn - for their guidance and support over these years. Truly an academic all-star team, I will continue to look up to each of them as models of scientific brilliance.

Thanks to all of the DAES faculty for building and carefully maintaining such a positive and constructive departmental culture. It was always comforting to know that every faculty member truly cared about the students, and always worked to build us up as scientists and professionals. Nowhere was their dedication to students more evident than in their outstanding courses, which I thoroughly enjoyed, and which greatly contributed to my knowledge.

I also owe a tremendous debt to Steven Lazarus and Michael Splitt of the Florida Institute of Technology, whose selfless investment in me as an undergraduate played a critical role in my academic development, and prepared me for PhD-level research and course work.

I am grateful for the support and friendship of all of the DAES graduate students,

particularly Travis Elless, Stephanie Stevenson, Oscar Chimborazo, Sarah Ditchek, Matthew Vaughan, and Steven Fuhrman. Their friendship and encouragement over these years has meant a lot to me. I owe a special thanks to Chip Helms for not only being a fantastic friend, but for innumerable stimulating conversations, and for introducing me to so many people in the tropical meteorology community. Thanks also to research associate Dave Vollaro, whose guidance during my first year of graduate school greatly accelerated my development as a programmer, and whose baseball knowledge far surpassed mine.

Last and most importantly, I thank my fiancée, Erika Navarro, for her constant love and support, and my parents for the innumerable sacrifices that they have made on my behalf. Their gentle encouragement always pushed me to achieve my greatest potential, and their belief in me provided indispensible sustenance during times of hardship. This work is dedicated to them.

CONTENTS

1. Introduction

1.1 Section Heading

I can reference a section using the label, for example: Section 1.

1.1.1 Subsection Heading

2. The tropopause-layer static stability structure of tropical cyclones: Idealized modeling

2.1 Introduction

The preceding two chapters highlighted the effect of tropical cyclones on the tropopause and upper-level static stability structure in dropsonde observations. These observations alone, however, cannot explain the mechanisms that force the observed variability. Numerical simulations of an axisymmetric hurricane conducted in an idealized framework reproduced the observed variability. Using these simulations, some physical insight into these mechanisms is obtained and described in the present chapter.

2.2 Model Setup

The numerical simulations were performed using version 19.4 of Cloud Model 1 (CM1) described in Bryan and Rotunno (2009). The equations of motion were integrated on a 3000-km-wide, 30-km-deep axisymmetric grid with 1-km horizontal and 250-m vertical grid spacing. The computations were performed on an f-plane at 15°N latitude, over a sea surface with constant temperature of 30.5°C, which matches that observed near Hurricane Patricia (2015; Kimberlain et al. 2016). Horizontal turbulence was parameterized using the Smagorinsky scheme described in Bryan and Rotunno (2009, pg. 1773), with a prescribed mixing length that varied linearly from 100 m at a surface pressure of 1015 hPa to 1000 m at a surface pressure of 900 hPa. Vertical turbulence was parameterized using the formulation of Markowski and Bryan (2016, their Eq. 6), using an asymptotic vertical mixing length of 100 m. A Rayleigh damping layer was applied outside of the 2900-km radius and above the 25-km level to prevent spurious gravity wave reflection at the model boundaries. Microphysical processes were parameterized using the Thompson et al. (2004) scheme and radiative heating tendencies were computed every two minutes using the Rapid Radiative Transfer Model for GCMs (RRTMG) longwave and shortwave schemes (Iacono et al. 2008). The initial

temperature and humidity field was horizontally homogeneous and determined by averaging all Climate Forecast System Reanalysis (CFSR) grid points within 100 km of Patricia's center of circulation at 18 UTC 21 October 2015. The vortex described in Rotunno and Emanuel (1987, their Eq. 37) was used to initialize the wind field, setting all parameters equal to the values used therein.

Although hurricanes simulated in an axisymmetric framework tend to be more intense than those observed in nature, the intensity evolution of this simulation matches reasonably well with that observed in Hurricane Patricia. After an initial spin-up period of about 20 hours, the modeled storm (Fig. 2.1, blue lines) began an RI period that lasted approximately 30 hours. After this RI, the storm continued to intensify more slowly until the maximum 10-m wind speed reached 89 m s^{-1} and the sea-level pressure reached its minimum of 846 hPa 81 hours into the simulation. Hurricane Patricia (red stars) exhibited a similar intensity evolution prior to its landfall, with an RI period leading to a maximum 10-m wind speed of 95 m s^{-1} and a minimum sea-level pressure of 872 hPa.

2.3 Budget Computation

The static stability can be expressed as the squared Brunt-Väisälä frequency:

$$N_m^2 = \frac{g}{T}\left(\frac{\partial T}{\partial z} + \Gamma_m\right)\left(1 + \frac{T}{R_d/R_v + q_s}\frac{\partial q_s}{\partial T}\right) - \frac{g}{1+q_t}\frac{\partial q_t}{\partial z}, \tag{2.1}$$

where g is gravitational acceleration, T is temperature, R_d and R_v are the gas constants of dry air and water vapor, respectively, q_s is the saturation mixing ratio, q_t is the total condensate mixing ratio, and Γ_m is the moist-adiabatic lapse rate:

$$\Gamma_m = g(1+q_t)\left(\frac{1 + L_v q_s/R_d T}{c_{pm} + L_v \partial q_s/\partial T}\right), \tag{2.2}$$

where L_v is the latent heat of vaporization and c_{pm} is the specific heat of moist air at constant pressure. In the tropopause layer, q_s, $\partial q_s/\partial T$, and $\partial q_t/\partial z$ approach zero. In this limiting

case, Eq. 2.1 reduces to:

$$N^2 = \frac{g}{\theta}\frac{\partial \theta}{\partial z}, \tag{2.3}$$

where θ is the potential temperature.

To compute N^2, CM1 uses Eq. 2.1 in saturated environments and Eq. 2.3 in sub-saturated environments. For simplicity, however, only Eq. 2.3 will be employed for the budget computations throughout the entire domain[1].

Taking the time derivative of Eq. 2.3 yields the static stability tendency:

$$\frac{\partial N^2}{\partial t} = \frac{g}{\theta}\frac{\partial}{\partial z}\frac{\partial \theta}{\partial t} - \frac{g}{\theta^2}\frac{\partial \theta}{\partial z}\frac{\partial \theta}{\partial t}, \tag{2.4}$$

where the potential temperature tendency, $\partial\theta/\partial t$, can be written, following Bryan (cited 2018):

$$\frac{\partial \theta}{\partial t} = -u\frac{\partial \theta}{\partial r} - w\frac{\partial \theta}{\partial z} + HTURB + VTURB + MP + RAD + DISS \tag{2.5}$$

Each term on the right-hand side of Eq. 2.5 represents a θ budget variable, each of which is output directly by the model every minute.

The first term on the right-hand side of Eq. 2.4 is larger than the second term throughout most of the tropopause layer (not shown). Consequently, the contribution of each of the terms in Eq. 2.5 to the N^2 tendency can be interpreted in light of a vertical gradient of each term.

Taking the vertical gradient of the first two terms on the right-hand side of Eq. 2.5 yields the time tendency of the vertical θ gradient due to horizontal and vertical advection[2]:

$$\left(\frac{\partial}{\partial t}\frac{\partial \theta}{\partial z}\right)_{adv} = -u\frac{\partial}{\partial r}\frac{\partial \theta}{\partial z} - w\frac{\partial}{\partial z}\frac{\partial \theta}{\partial z} - \frac{\partial u}{\partial z}\frac{\partial \theta}{\partial r} - \frac{\partial w}{\partial z}\frac{\partial \theta}{\partial z}. \tag{2.6}$$

The first two terms on the right-hand side of Eq. 2.6 represent advection of static stability by

[1] The validity of this approximation will be substantiated later in this section.

[2] These terms include the tendencies due to implicit diffusion in the fifth-order finite differencing scheme, which are separated from the advection terms in the CM1 version 19.4 budget output.

the radial and vertical wind, respectively. These terms act to rearrange the static stability field, but cannot strengthen or weaken static stability maxima or minima. The third and fourth terms on the right-hand side of Eq. 2.6 represent, respectively, the tilting of isentropes in the presence of vertical wind shear, and the stretching or squashing of isentropes by vertical gradients of vertical velocity. Since these terms involve velocity gradients, they can act to strengthen or weaken static stability maxima or minima through differential advection. Unless otherwise stated, any reference to "advection" in this paper indicates the sum of all of the terms in Eq. 2.6.

Returning to Eq. 2.5, HTURB and VTURB are the θ tendencies from the horizontal and vertical turbulence parameterizations, MP is the tendency from the microphysics scheme, RAD is the tendency from the radiation scheme, and DISS is the tendency due to turbulent dissipation. This equation neglects Rayleigh damping, since the entire analysis domain lies outside of the regions where damping is applied. Each term in Eq. 2.5 is substituted for $\partial\theta/\partial t$ in Eq. 2.4, yielding the contribution of each budget term to the static stability tendency. These terms are summed, yielding an instantaneous "budget change" in N^2 every minute. The budget changes are then averaged over 24-hour periods and compared to the total model change in N^2 over that same time period, i.e.:

$$\Delta N^2_{budget} = \frac{1}{\delta t} \sum_{t=t_0}^{t_0+\delta t} \left. \frac{\partial N^2}{\partial t} \right|_t \tag{2.7}$$

$$\Delta N^2_{model} = N^2_{t_0+\delta t} - N^2_{t_0} \tag{2.8}$$

$$Residual = \Delta N^2_{model} - \Delta N^2_{budget} \tag{2.9}$$

where t_0 is an initial time and δt is 24 hours.

Eqs. 2.7-2.9 are plotted for three consecutive 24-hour periods in Fig. 2.2. For this and all subsequent radial-vertical cross sections, a 1-2-1 smoother is applied once in the radial direction to eliminate $2\Delta r$ noise that appears in some of the raw model output and calculated

fields. The left column of Fig. 2.2 depicts the model changes computed using Eq. 2.8, together with Eq. 2.1 in saturated environments and Eq. 2.3 in subsaturated environments. The center column depicts the budget changes computed using Eq. 2.7 together with Eq. 2.3 throughout the entire domain. Thus, the left column includes the effect of moisture in the N^2 computations, whereas the center column neglects moisture. The right column depicts the residuals, computed using Eq. 2.9 (i.e. the left column minus the center column.) In every 24-hour period, the budget changes are nearly identical to the model changes, which is reflected in the near-zero residuals in the right column. This indicates that the budget accurately represents the model variability, which implies that the neglect of moisture in the budget computation introduces negligible error within the analysis domain[3].

In the tropopause layer, some of the budget terms are small enough to be ignored. To determine which of the budget terms are most important, a time series of the contribution of each of the budget terms in Eq. 2.5 to the tropopause-layer static stability tendency is plotted in Fig. 2.3. For this figure, each of the budget terms is computed using the method described in Section 3, except with 1-hour averaging intervals instead of 24-hour intervals. The absolute values of these tendencies are then averaged over the radius-height domain of the plots shown in Fig. 2.2 and plotted as a time series[4]. Advection (Fig. 2.3, red line) plays an important role in the mean tropopause-layer static stability tendency at all times, and vertical turbulence (Fig. 2.3, blue line) and radiation (Fig. 2.3, dark green line) also contribute significantly. The remaining three processes - horizontal turbulence, microphysics, and dissipative heating - are negligible everywhere outside of the eyewall, and do not play important roles in the mesoscale tropopause variability.

The preceding analysis indicates that, at all times, three budget terms dominate the

[3] This is not the case in the lower- and mid-troposphere, where the residual actually exceeds the budget tendencies in many places, likely due to the neglect of moisture; thus we limit this analysis to the upper troposphere and lower stratosphere.

[4] It will be seeen in subsequent figures that each of the terms contributes both positively and negatively to the N^2 tendency within the analysis domain. Thus, taking an average over the domain tends to wash out the positive and negative contributions. To circumvent this problem, the absolute value of each of the terms is averaged.

tropopause-layer static stability tendency: advection, vertical turbulence, and radiation. Variations in the magnitude and spatial structure of these terms drive the static stability changes depicted in Fig. 2.2; subsequent sections will focus on these variations and what causes them.

2.4 Results

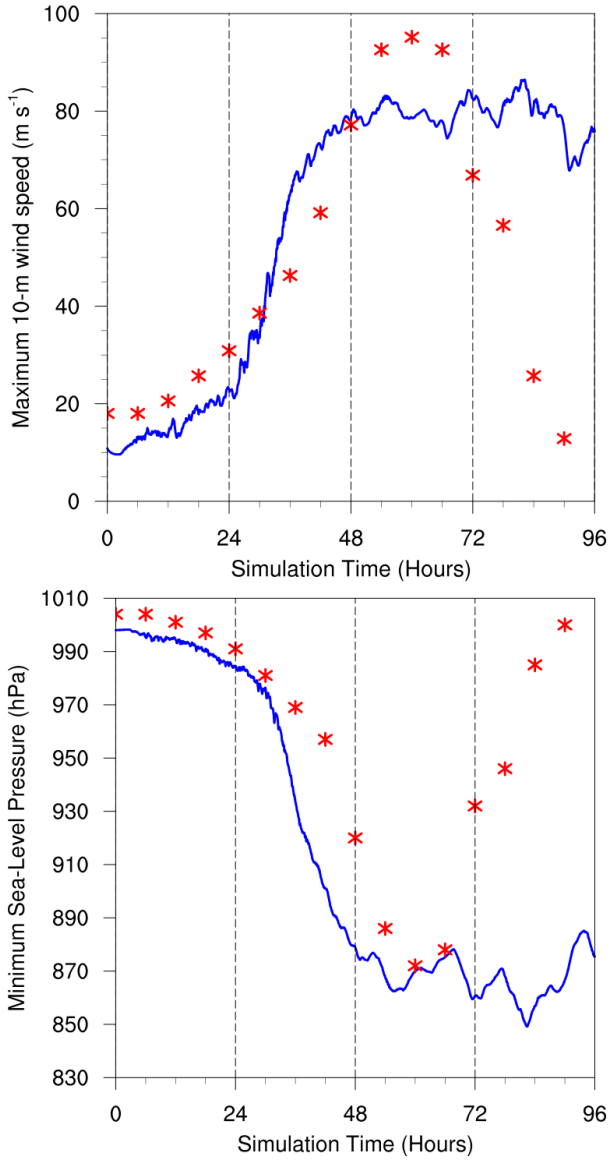

Figure 2.1: The maximum 10-m wind speed (top panel; m s^{-1}) and minimum sea-level pressure (bottom panel; hPa) in the simulated storm (blue lines; plotted every minute) and from Hurricane Patricia's best track (red stars; plotted every six hours beginning at the time Patricia attained tropical storm intensity). The rapid weakening during the later stage of Patricia's lifetime was induced by landfall.

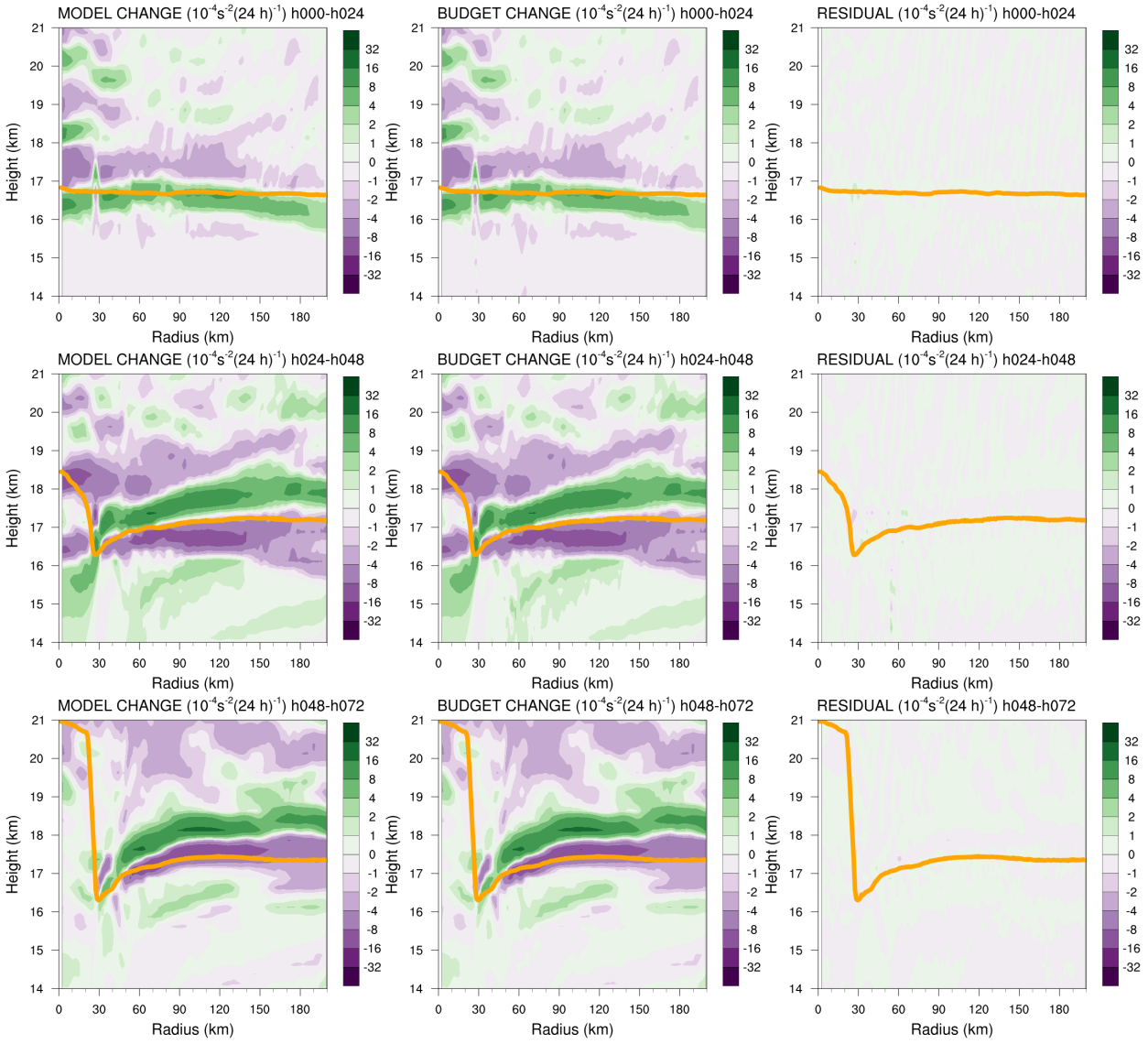

Figure 2.2: Left panels: Twenty-four-hour changes in squared Brunt-Väisälä frequency (N^2; 10^{-4} s^{-2}) computed using Eq. 2.8 over (top row) 0-24 hours, (middle row) 24-48 hours, (bottom row) 48-72 hours. Middle Panels: The N^2 change over the same time periods computed using Eqs. 2.4-2.7, Right Panels: The budget residual over the same time periods, computed by subtracting the budget change (middle column) from the model change (left column). Orange lines represent the cold-point tropopause height averaged over the same time periods.

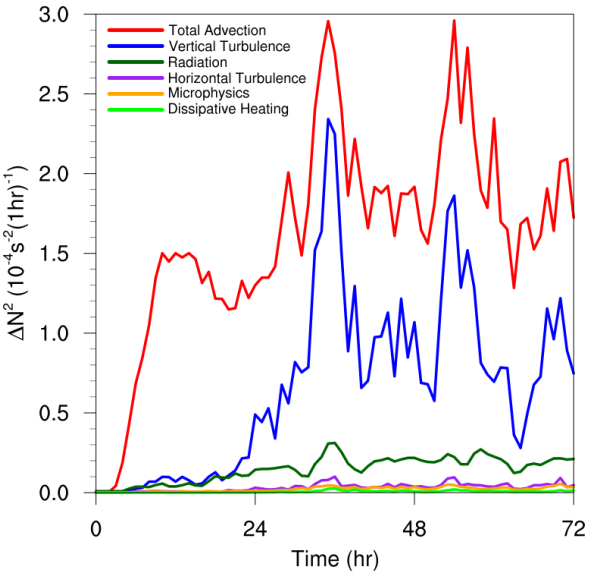

Figure 2.3: Time series of the contribution of each of the budget terms to the time tendency of the squared Brunt-Väisälä frequency (N^2; 10^{-4} s^{-2}). For each budget term, the absolute value of the N^2 tendency is averaged temporally over 1-hour periods (using output every minute), and spatially in a region extending from 0 to 200 km radius and 14 to 21 km altitude.

BIBLIOGRAPHY

Bryan, G. H., cited 2018: The governing equations for CM1. [Available online at http://www2.mmm.ucar.edu/people/bryan/cm1/cm1_equations.pdf].

Bryan, G. H., and R. Rotunno, 2009: The maximum intensity of tropical cyclones in axisymmetric numerical model simulations. *Mon. Wea. Rev.*, **137 (6)**, 1770–1789.

Iacono, M. J., J. S. Delamere, E. J. Mlawer, M. W. Shephard, S. A. Clough, and W. D. Collins, 2008: Radiative forcing by long-lived greenhouse gases: Calculations with the AER radiative transfer models. *J. Geophys. Res.*, **113 (D13103)**.

Kimberlain, T. B., E. S. Blake, and J. P. Cangialosi, 2016: Tropical cyclone report: Hurricane Patricia. National Hurricane Center. [Available online at www.nhc.noaa.gov].

Markowski, P. M., and G. H. Bryan, 2016: LES of laminar flow in the PBL: A potential problem for convective storm simulations. *Mon. Wea. Rev.*, **144**, 1841–1850.

Rotunno, R., and K. A. Emanuel, 1987: An air-sea interaction theory for tropical cyclones. Part II: Evolutionary study using a nonhydrostatic axisymmetric numerical model. *J. Atmos. Sci.*, **44**, 542–561.

Thompson, G., R. M. Rasmussen, and K. Manning, 2004: Explicit Forecasts of Winter Precipitation Using an Improved Bulk Microphysics Scheme. Part I: Description and Sensitivity Analysis. *Mon. Wea. Rev.*, **132 (2)**, 519–542.